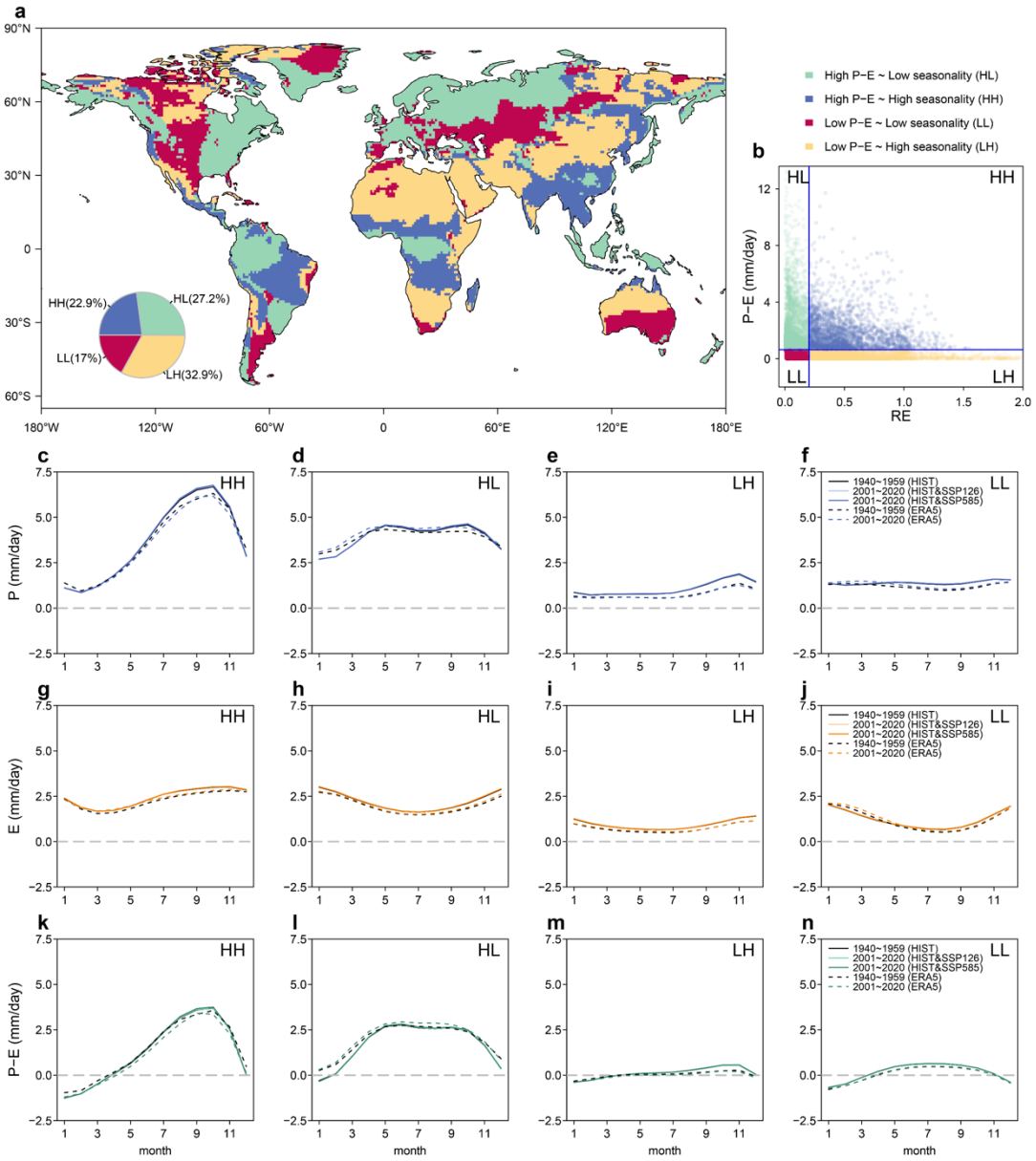

Figure S1. Global distribution of hydroclimate regimes based on the ERA5 reanalysis. (a) The global distribution of four hydroclimate regimes based on the median (i.e., 50th percentile) thresholds of the mean water availability (P-E) and relative entropy (RE) of precipitation from the ERA5 reanalysis during 1971-2000. The pie plot insets show the proportion of land areas for the four regimes. The first letter represents the high (H) or low (L) level of the mean P-E and the second letter for the level of hydroclimate seasonality. (b) Distribution of the mean P-E and RE across land grid cells, and the median thresholds are shown as blue lines. (c-f) Monthly mean precipitation (P) in the four regimes during the periods of 1940-1959 and 2001-2020 based on the ERA5 reanalysis and the historical and future (ssp1-2.6 and ssp5-8.5) simulations of CMIP6 models. (g-n) the same as (c-f), but for evaporation (E, g-j), and surface water availability (P-E, k-n). Month 1 along the x-axis is associated with the month with the lowest P-E during the historical period.

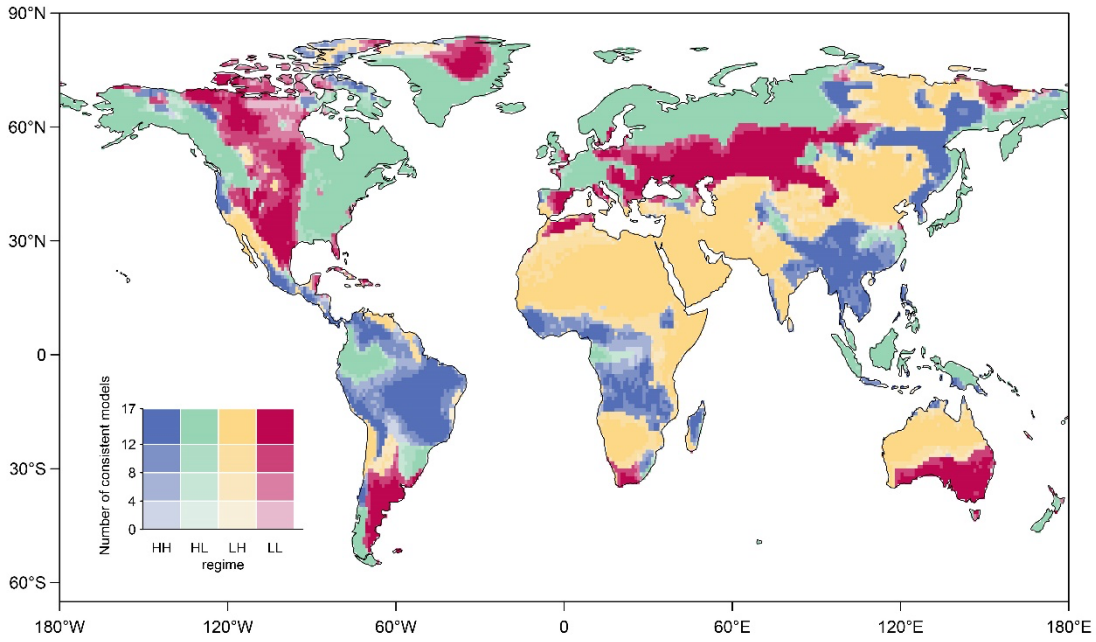

Figure S2. Multi-model consistency in the global distribution of hydroclimate regimes as shown in Fig. 1a.

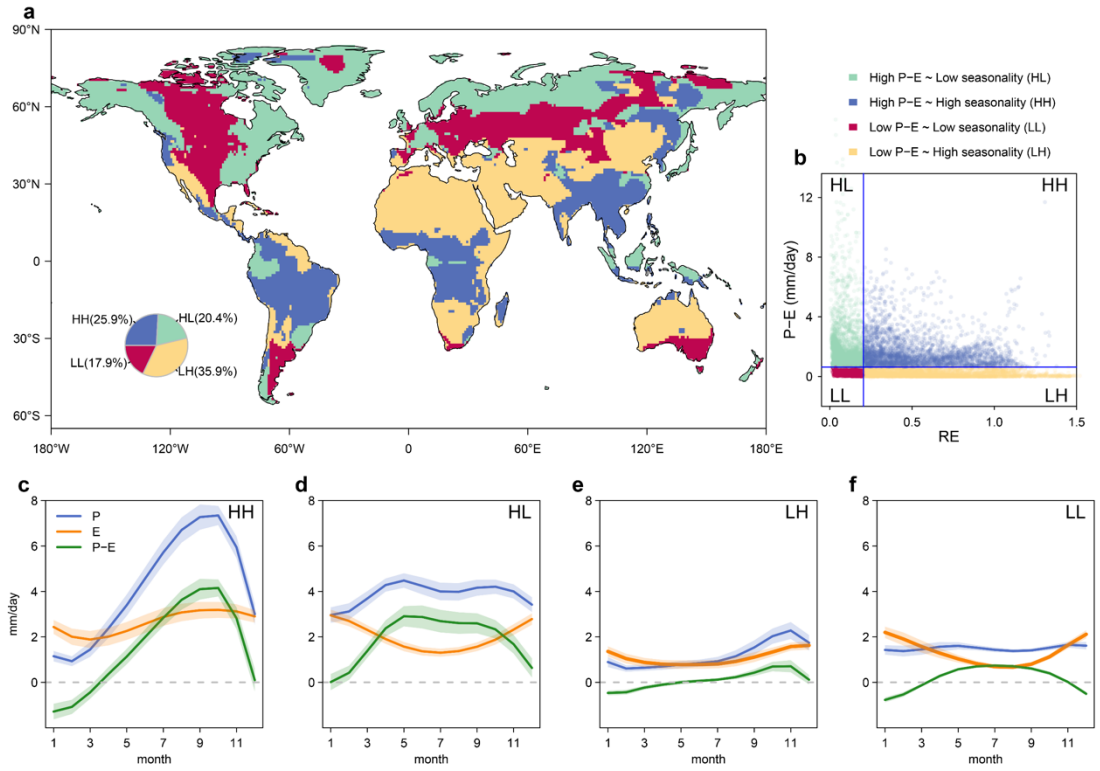

Figure S3. Global distribution of hydroclimate regimes in future projections. (a) The global distribution of four hydroclimate regimes based on the median (i.e., 50th percentile) thresholds of the multi-model mean water availability (P-E) and relative entropy (RE) of precipitation during the future period (2071-2100, ssp5-8.5). The pie plot insets show the proportion of land areas for the four regimes. The first letter represents the high (H) or low (L) level of the mean P-E and the second letter for the level of hydroclimate seasonality. (b) Distribution of the multi-model mean P-E and RE across land grid cells, and the median thresholds are shown as blue lines. (c-f) Multi-model mean precipitation (P), evaporation (E), and surface water availability (P-E) in the regime HH (c), HL (d), LH (e), and LL (f). The shading shows the standard deviation of the hydroclimate variables across the 17 climate models. Month 1 along the x-axis is associated with the month with the lowest P-E during the historical period.

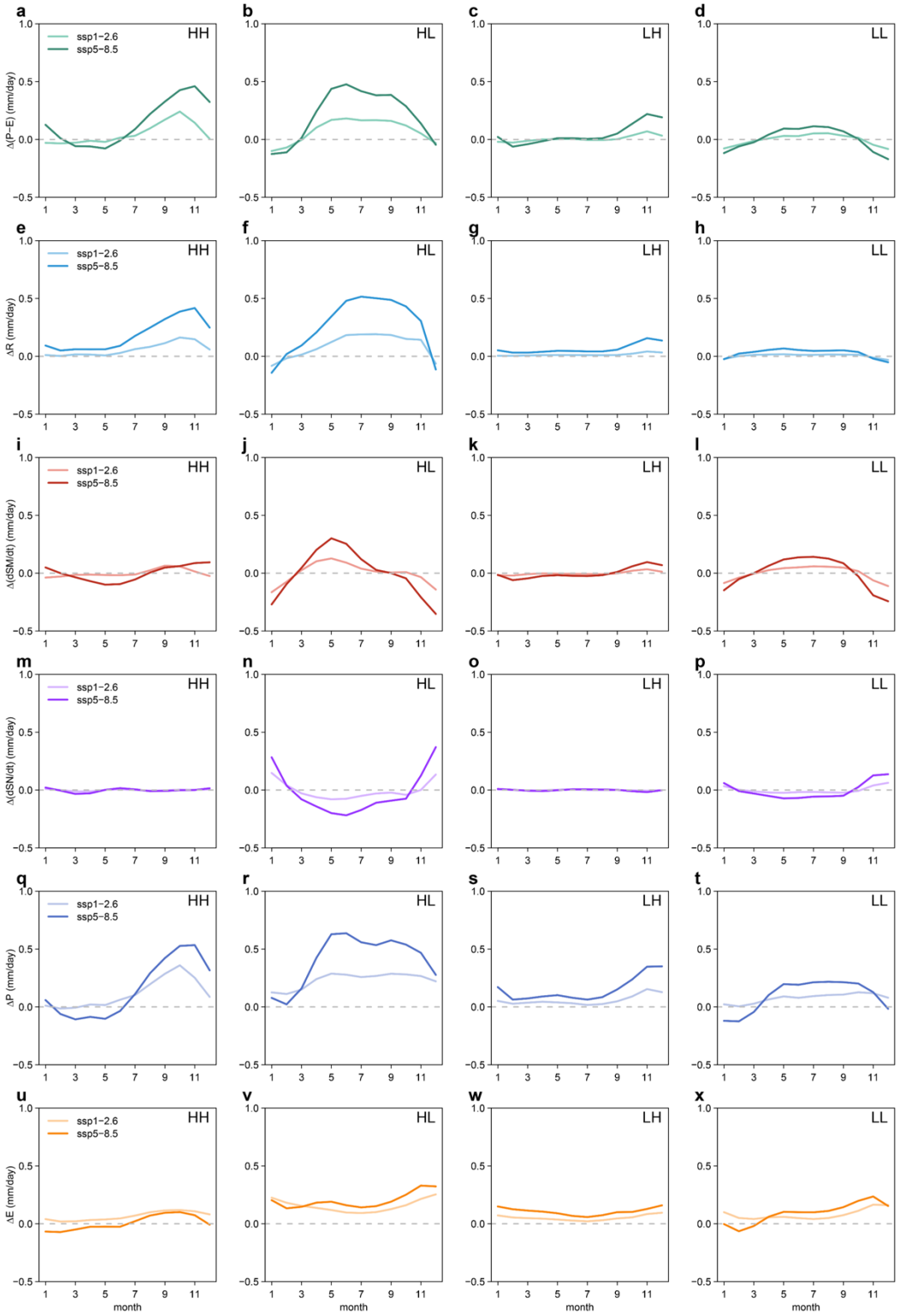

Figure S4. Multi-model mean seasonal changes of terrestrial water balance for the four hydroclimate regimes. The same as Fig. 2d-s and Fig. 4g-n, but for net changes in P-E (a-d), R (e-h), dSM/dt (i-l), dSN/dt (m-p), P (q-t), and E (u-x) between the historical (1971-2000) and future (ssp1-2.6 or ssp5-8.5, 2071-2100) periods (future minus historical values). Month 1 along the x-axis is associated with the month with the lowest P-E during the historical period.

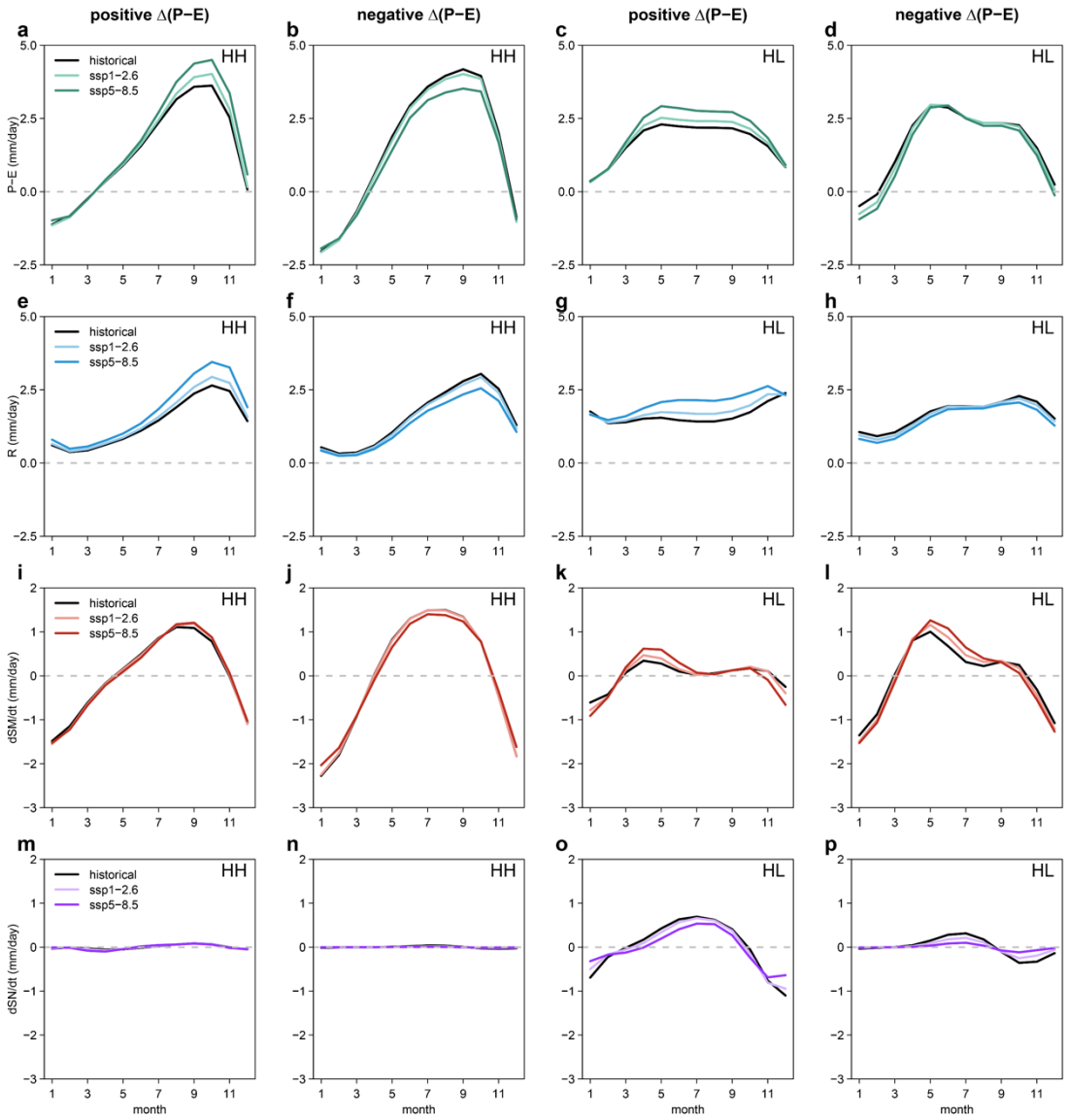

Figure S5. Future shifts in the mean seasonal cycles of terrestrial water balance for regimes HH and HL. (a-d) The same as Fig. 2d,e, but for HH and HL areas where water availability increases (i.e., positive Δ(P-E)) and decreases (i.e., negative Δ(P-E)), respectively, from the historical (1971-2000) to future (ssp5-8.5, 2071-2100) periods. (e-p) The same as a-d, but for the mean seasonal cycles of runoff (R, e-h), changes in soil moisture (dSM/dt, i-l) and snow amount (dSN/dt, m-p) over time, for HH and HL areas with positive and negative Δ(P-E). Month 1 along the x-axis is associated with the month with the lowest P-E during the historical period.

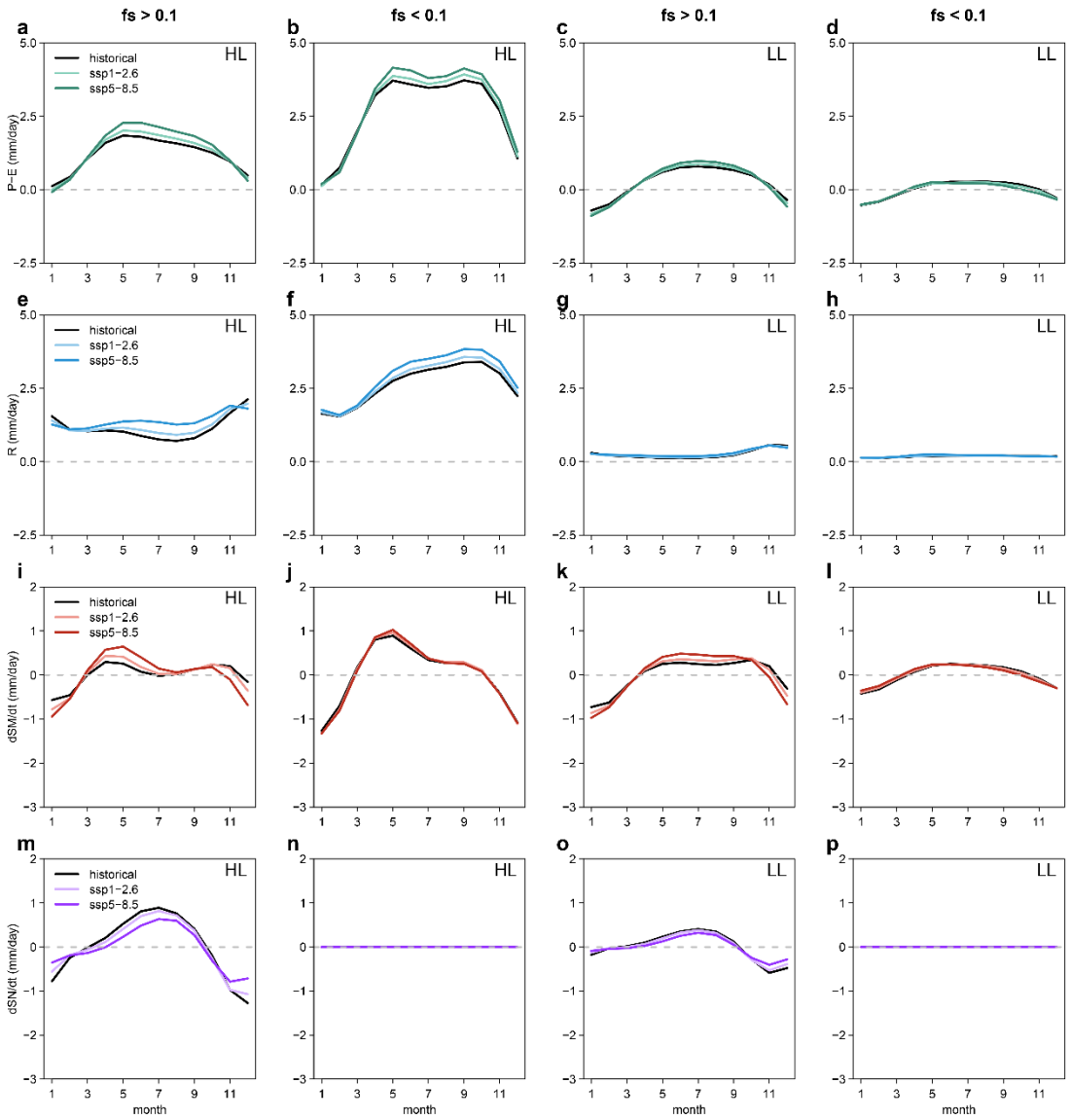

Figure S6. Future shifts in the mean seasonal cycles of terrestrial water balance for regimes HL and LL. (a-d) The same as Fig. 2d,e, but for HL and LL areas where the mean annual snowfall fraction of precipitation (fs) is higher (snow-covered regions) and lower (snow-free regions) than 0.1, respectively, from the historical (1971-2000) to future (ssp5-8.5, 2071-2100) periods. (e-p) The same as a-d, but for the mean seasonal cycles of runoff (R, e-h), changes in soil moisture (dSM/dt, i-l) and snow amount (dSN/dt, m-p) over time, for HL and LL areas. Month 1 along the x-axis is associated with the month with the lowest P-E during the historical period.

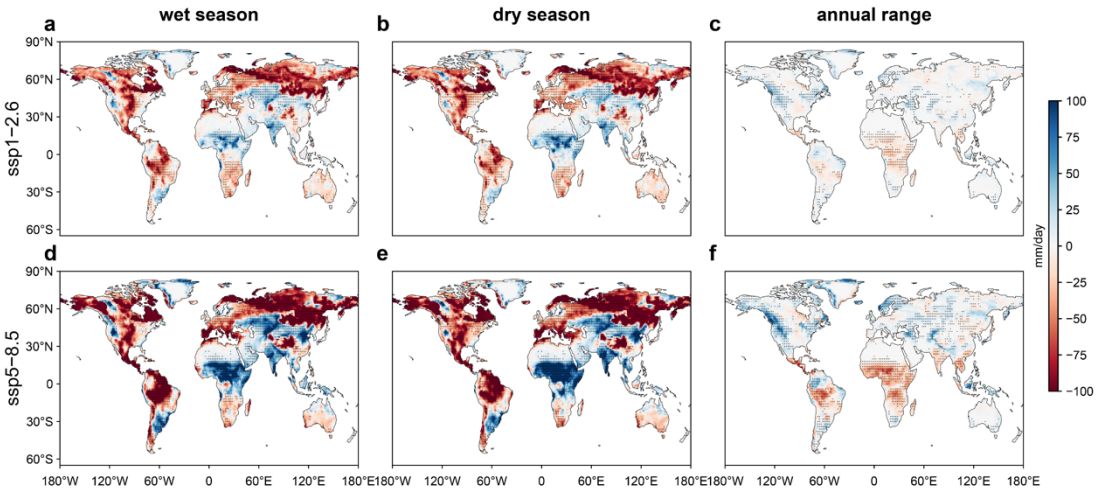

Figure S7. Multi-model mean seasonal changes in soil moisture between the historical and future periods. (a-c) Changes in soil moisture (ΔSM) in the wet season (a) and the dry season (b), and their differences (i.e., the annual range of SM, c) between the historical (1971-2000) and future (2071-2100, ssp1-2.6) periods. (d-f) The same as a-c, but for the differences between the historical and ssp5-8.5 scenarios. The dotted areas denote the sign of ΔSM is consistent with the sign of multi-model mean ΔSM for more than 75% (at least 13) of the 17 models.

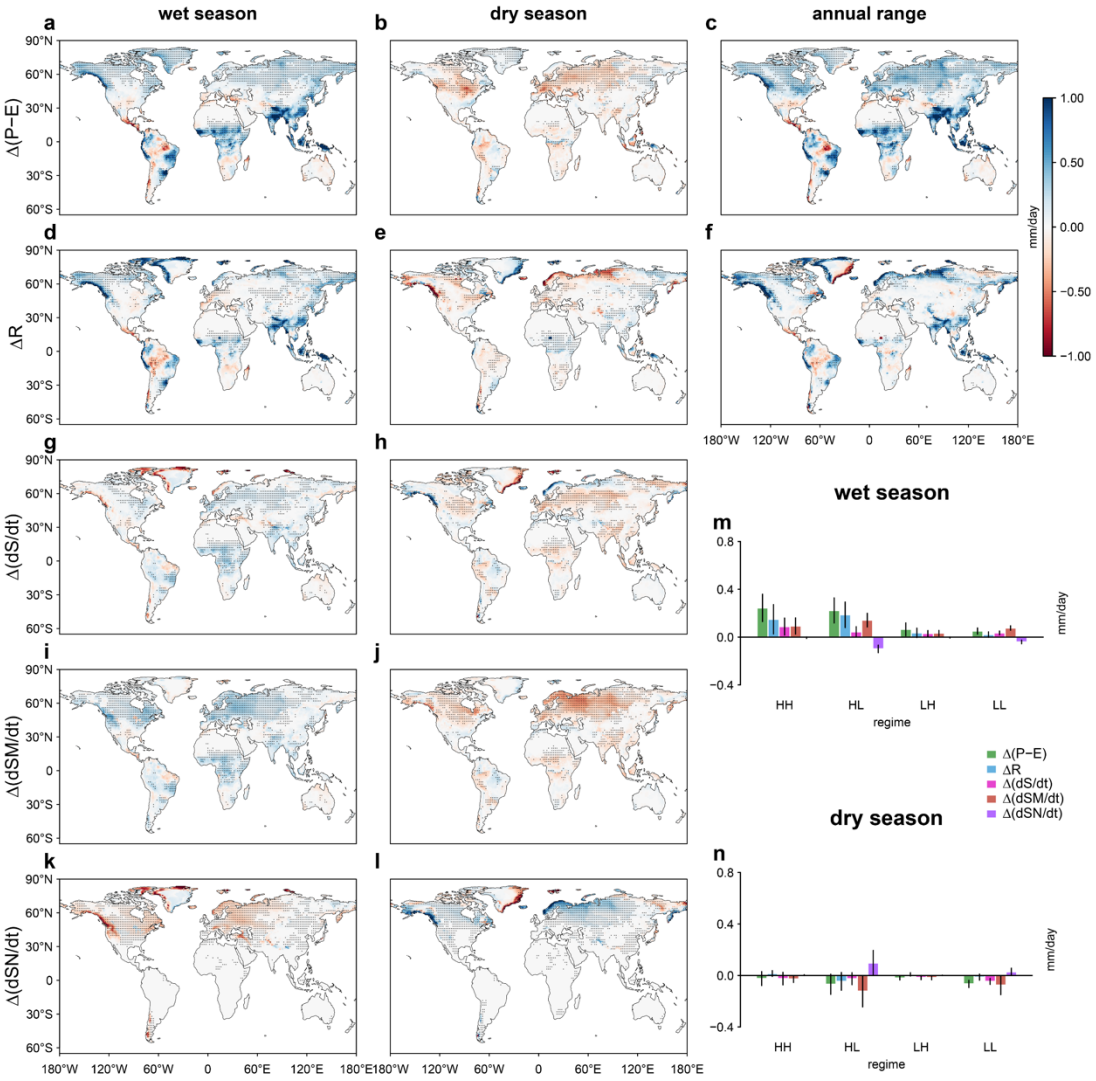

Figure S8. Multi-model mean seasonal changes in water availability between the historical and future periods. (a-c) Changes in water availability (Δ(P-E)) in the wet season (a) and the dry season (b), and their differences (i.e., the annual range of P-E, c) between the historical (1971-2000) and future (2071-2100, ssp1-2.6) periods. (d-l) The same as a-c, but for runoff (R, d-f), changes in water storage (dS/dt, g,h), soil moisture (dSM/dt, i,j), and snow amount (dSN/dt, k,l) over time during the wet and dry seasons. The dotted areas denote the sign of changes in the variables is consistent with the sign of multi-model means for more than 75% (at least 13) of the 17 models. (m,n) The area-weighted mean Δ(P-E), ΔR, Δ(dS/dt), Δ(dSM/dt) and Δ(dSN/dt) for the four regimes between the historical and future periods. The error bars show the standard deviations of the variables across the 17 models.

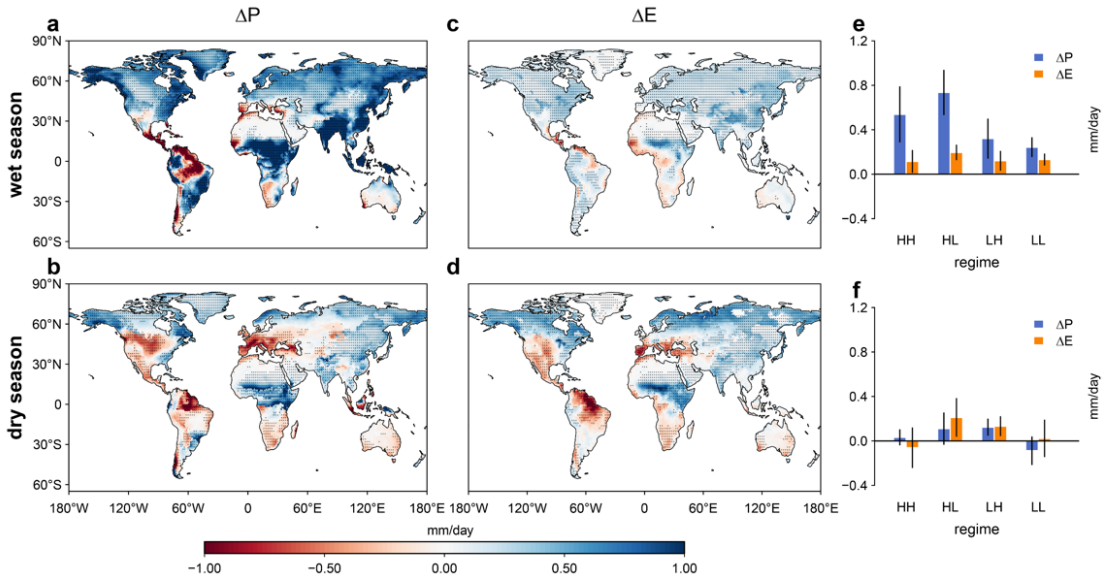

Figure S9. Multi-model mean seasonal changes in precipitation and evapotranspiration between the historical and future periods. (a-b) Changes in precipitation (ΔP) in the wet season (a) and the dry season (b) between the historical (1971-2000) and future (2071-2100, ssp5-8.5) periods. (c-d) The same as a-b, but for changes in evapotranspiration (ΔE). The dotted areas denote the sign of ΔP or ΔE is consistent with the sign of multi-model means for more than 75% (at least 13) of the 17 models. (e-f) The area-weighted mean ΔP and ΔE for the four regimes between the historical and future periods. The error bars show the standard deviations of ΔP and ΔE across the 17 models.

Table S1. List of the 17 CMIP6 models used in this study.

No.	Model	Ensemble	Spatial Resolution (Lon. x Lat.)	Modeling Center
1	ACCESS-CM2	r1i1p1f1	1.9°×1.3°	Commonwealth Scientific and Industrial Research Organization (CSIRO) Australian Research Council Centre of Excellence for Climate System Science (ARCCSS)
2	ACCESS-ESM1-5	r1i1p1f1	1.9°×1.2°	Commonwealth Scientific and Industrial Research Organization (CSIRO)
3	CESM2-WACCM	r1i1p1f1	1.3°×0.9°	National Center for Atmospheric Research (NCAR)
4	CNRM-CM6-1	r1i1p1f2	1.4°×1.4°	Centre National de Recherches Météorologiques (CNRM) Centre Européen de Recherche et Formation Avancée en Calcul Scientifique (CERFACS)
5	CNRM-CM6-1-HR	r1i1p1f2	0.5°×0.5°	
6	CNRM-ESM2-1	r1i1p1f2	1.4°×1.4°	
7	EC-EARTH3	r1i1p1f1	0.7°×0.7°	EC-EARTH consortium
8	EC-EARTH3-Veg	r1i1p1f1	0.7°×0.7°	
9	HadGEM3-GC31-LL	r1i1p1f3	1.9°×1.3°	Met Office Hadley Centre (MOHC) Natural Environment Research Council (NERC)
10	HadGEM3-GC31-MM	r1i1p1f3	0.8°×0.6°	
11	IPSL-CM6A-LR	r1i1p1f1	2.5°×1.3°	Institut Pierre Simon Laplace (IPSL)
12	MIROC6	r1i1p1f1	1.4°×1.4°	Japan Agency for Marine-Earth Science and Technology (JAMSTEC) Atmosphere and Ocean Research Institute (AORI) National Institute for Environmental Studies (NIES) RIKEN Center for Computational Science (RCCS)
13	MIROC-ES2L	r1i1p1f2	2.8°×2.8°	
14	MPI-ESM1-2-HR	r1i1p1f1	0.9°×0.9°	Max Planck Institute for Meteorology (MPI-M) Deutscher Wetterdienst (DWD) Deutsches Klimarechenzentrum (DKRZ)
15	MPI-ESM1-2-LR	r1i1p1f1	1.9°×1.9°	
16	MRI-ESM2-0	r1i1p1f1	1.1°×1.1°	Meteorological Research Institute (MRI)
17	UKESM1-0-LL	r1i1p1f2	1.9°×1.3°	Met Office Hadley Centre (MOHC) Natural Environment Research Council (NERC) National Institute of Meteorological Sciences/Korea Meteorological Administration (NIMS-KMA) National Institute of Water and Atmospheric Research (NIWA)